

Modelling detrital cooling-age populations: insights from two Himalayan catchments

I. D. Brewer,* D. W. Burbank† and K. V. Hodges‡

*Department of Geosciences, The Pennsylvania State University, University Park, Pennsylvania, USA

†Department of Geological Sciences, University of California, Santa Barbara, California, USA

‡Department of Earth, Atmospheric, and Planetary Sciences, Massachusetts Institute of Technology, Cambridge, Massachusetts, USA

ABSTRACT

The distribution of detrital mineral cooling ages in river sediment provides a proxy record for the erosional history of mountain ranges. We have developed a numerical model that predicts detrital mineral age distributions for individual catchments in which particle paths move vertically toward the surface. Despite a restrictive set of assumptions, the model permits theoretical exploration of the effects of thermal structure, erosion rate, and topography on cooling ages. Hypsometry of the source-area catchment is shown to exert a fundamental control on the frequency distribution of bedrock and detrital ages. We illustrate this approach by generating synthetic $^{40}\text{Ar}/^{39}\text{Ar}$ muscovite age distributions for two catchments with contrasting erosion rates in central Nepal and then by comparing actual measured cooling-age distributions with the synthetic ones. Monte Carlo sampling is used to assess the mismatch between observed and synthetic age distributions and to explore the dependence of that mismatch on the complexity of the synthetic age signal and on the number of grains analysed. Observed detrital cooling ages are well matched by predicted ages for a more slowly eroding Himalayan catchment. A poorer match for a rapidly eroding catchment may result from some combination of large analytical uncertainties in the detrital ages and inhomogeneous erosion rates within the basin. Such mismatches emphasize the need for more accurate thermal and kinematic models and for sampling strategies that are adapted to catchment-specific geologic and geomorphic conditions.

INTRODUCTION

In active tectonic terrains, cooling rates obtained through the application of isotope thermochronometers are frequently used as proxies for erosion rates. Conversion of a cooling age into an erosion rate commonly utilizes several either implicit or explicit assumptions, including: (a) a specified geothermal gradient; (b) constant erosion rate through time; and (c) vertical rock-particle trajectories. Such an approach often ignores natural complexities, such as the influence of topographic relief, erosion rate, and deformation on thermal structure and erosional histories (Stüwe *et al.*, 1994; Henry *et al.*, 1997; Mancktelow & Grasemann, 1997; Stüwe & Hintermüller, 2000). This study explores some of the basic assumptions required to calculate erosion rates, investigates the interplay of parameters that control the distribution of bedrock-cooling ages, and examines the impact of sampling strategies on observed cooling-age distributions.

Temperature-through-time cooling paths for bedrock samples can be reconstructed through the successful application of multiple thermochronometric techniques. Although detailed studies on individual samples can provide a rich cooling history, such studies commonly provide data on a few discrete points in a landscape and are restricted to existing bedrock in outcrop or boreholes. In contrast, a handful of sand collected at the mouth of a river can contain a half million grains extracted from throughout the upstream catchment, including areas characterized by glaciation or extreme relief: conditions that commonly thwart direct sampling of the bedrock. Thermochronologic studies of such detrital samples can potentially encapsulate the full spectrum of bedrock cooling ages in a catchment (Brandon & Vance, 1992; Garver *et al.*, 1999). Moreover, detrital dating studies can exploit the extensive temporal record of detritus shed from mountain belts and preserved in sedimentary basins.

Previously, detrital mineral thermochronology has been used to investigate: (a) the thermal evolution of basins (Brandon & Vance, 1992); (b) source-area characteristics (Krogh *et al.*, 1987; Hurford & Carter, 1991; Garver & Brandon, 1994; Adams *et al.*, 1998); (c) stratigraphic age (McGouldrick & Gleadow, 1978; Najman *et al.*, 1997); and (d) the

Correspondence: D. W. Burbank, Department of Geological Sciences, University of California, Santa Barbara, CA 93106, USA. E-mail: burbank@crustal.ucsb.edu

erosional and tectonic history of orogens (Cerveny *et al.*, 1988; Copeland & Harrison, 1990; Garver & Brandon, 1994; Bernet *et al.*, 2001; White *et al.*, 2002). Among the earliest low-temperature detrital age studies, Cerveny *et al.* (1988) and Copeland & Harrison (1990) assumed that newly eroded detritus has a brief residence time in the sediment-transport system, so that the difference between cooling and depositional ages (the 'lag time') can be used to estimate hinterland erosion rates. Comparisons through time of the difference between cooling and depositional ages have been more recently used to assess thermal steady state in orogens (Bernet *et al.*, 2001), whereas downstream changes in detrital age populations have been exploited to examine mixing of source areas with different cooling ages (Bernet *et al.*, in press). These recent studies have focused on characterization of statistical components of the detrital age spectrum (Brandon, 1992, 2002) within a sample in order to identify peaks in age frequencies that can be correlated or compared among samples or to source areas. They have not explored the controls and character of the distribution of ages within a given source area: the focus of this study.

Several thermochronologic studies have shown that, for any given erosion rate, topographic relief will produce a spectrum of ages and deflect isotherms (Henry *et al.*, 1997; Mancktelow & Grasemann, 1997; Stüwe & Hintermüller, 2000). This natural variability commonly introduces unknown complexity into the interpretation of detrital ages derived from the stratigraphic record, because relief in the hinterland is unknown. Stock & Montgomery (1996) investigated the inverse problem from a theoretical perspective: using the detrital cooling-age signal in basins to constrain paleotopography with the assumption of accurate detrital grain ages, well-mixed sediment within basins, and horizontal isotherms. They found that a sample of 40 grains is required to provide a 90% probability of capturing 90% of the relief of a basin. We use a similar, but more integrated, approach to try to understand the thermal framework, topographic characteristics, and sampling statistics that control the complete cooling-age signal from a particular source-area catchment.

We introduce a two-part numerical model that explores the detrital cooling-age signal of a river catchment. Initially, a combination of erosion rate and relief is input to predict thermal structure and the consequent distribution of ages with elevation (e.g. Stüwe & Hintermüller, 2000). Based on catchment hypsometry (distribution of area with elevation), the model then predicts the theoretical distribution of detrital cooling ages that should reproduce the variability of bedrock cooling ages within the catchment and explores the impact of different hypsometric end-member geometries on predicted age distributions.

The second part of the model evaluates the consequences of the practical fact that we can date only a finite number of grains, such that a random suite of ages is drawn from a much larger distribution. Increasing the number of dated grains produces more robust analyses, but how can

we quantify this and balance it against the practicality that rather restricted numbers of grains are commonly dated? The problem of detecting the component peaks within a broader age distribution has been addressed previously using Gaussian-kernel functions (Brandon, 1992, 1996, 2002). Here, we introduce a method using Monte Carlo integration to generate synthetic 'grab' samples of finite size from known 'theoretical' populations to quantify how different age distributions, generated from different individual samples, fit a theoretical cooling-age signal. To compare model results to real data, we present detrital muscovite ages from two Himalayan catchments in central Nepal and use these to assess the assumptions and applicability of these models.

PREDICTING THE DISTRIBUTION OF BEDROCK COOLING AGES

Our model focuses on $^{40}\text{Ar}/^{39}\text{Ar}$ dating of muscovite because this thermochronologic approach has been widely used in investigations of both bedrock and detrital mineral dating. For our purposes, we assume that all muscovite grains have the same closure temperature ($\sim 350^\circ\text{C}$) and ignore the potential effects on closure temperature exerted by grain size, composition, inherited radiogenic ^{40}Ar , and the rate of cooling through the closure interval (see Dodson, 1973). For the applicable rates of cooling in this study ($\sim 10\text{--}100^\circ\text{C Myr}^{-1}$), the effective closure temperature could vary between 330°C and 400°C . The choice of 350°C represents a necessary compromise in the absence of detailed information on individual samples. Such data are commonly impractical to obtain in single-grain analyses of detrital grains.

Tectonic-erosion model

In active orogenic belts, cooling ages are determined by the thermal structure, which determines the depth of the mineral closure temperature, and particle velocities that determine how long rocks take to be transported from the closure temperature to the land surface, i.e. the cooling age. The majority of thermochronological investigations assume a simplified kinematic geometry such that rocks pursue a vertical trajectory towards the surface, with erosion occurring perpendicular to that path. Thus calculations based on vertical erosion typically simplify more complex processes involving lateral advection that are driven by horizontal shortening (Batt & Brandon, 2002; Willert & Brandon, 2002). Lateral advection usually lengthens the path that a thermochronometer takes to the surface. Hence, the particle travels further than estimated with solely vertical transportation, and, to the extent that the orogenic surface departs from horizontal, cooling ages could misestimate erosion rates. Nevertheless, for the purposes of this paper, particle trajectories and erosion are assumed to be 1-D processes such that an average erosion rate

(dz/dt) may be calculated from:

$$\frac{dz}{dt} = \frac{(T_c - T_s)}{(dT/dz)} \left(\frac{1}{t_c} \right) \quad (1)$$

where T_c is the closure temperature of the thermochronometer, T_s is the surface temperature, dT/dz is an assumed geothermal gradient and t_c is the closure age of the mineral.

Isothermal geometry

Differential deflection of isotherms due to relief and various erosion rates has been well established in theoretical models (Stüwe *et al.*, 1994; Mancktelow & Grasemann, 1997). We apply a similar methodology to approximate the 2-D, steady-state thermal structure using a 2-D combined diffusion and advection finite-difference scheme (Fletcher, 1991). Rather than the more commonly modelled sinusoidal topography, however, we specify linear hillslopes at 30° angles that are intended to approximate slope angles near the threshold for failure (Burbank *et al.*, 1996; Montgomery & Brandon, 2002). We also specify an average surface heat flow of $57 \times 10^{-3} \text{ W m}^{-2}$, uniform radioactive heat production of $1.0 \times 10^{-6} \text{ W m}^{-3}$ (Fowler, 1990), a surface temperature (T_s) of 20° C at the valley floor (as is appropriate for the subtropics), and an atmospheric adiabatic lapse rate of $6.5^\circ \text{ C km}^{-1}$ (Bloom, 1998). Spatially uniform erosion is simulated by the vertical advection of rock through steady-state topography that is generated instantaneously after $t > t_0$. The model defines the position and shape of the 350° C isotherm as a function of various topographic configurations and erosion rates.

Consistent with previous results, our model predicts that increasing relief causes greater deflection of isotherms from their original horizontal orientation and that, as erosion rates increase, all isotherms move closer to the surface. Relief causes the maximum deflection of the lowest temperature isotherms. For topographic relief of $\leq 6 \text{ km}$ and for erosion rates $\leq 3 \text{ km Myr}^{-1}$; however, the 350° C isotherm develops a maximum of only 400 m of relief over 20 km wavelengths. For the purposes of our modelling and because we do not consider erosion rates exceeding 3 km Myr^{-1} , we consequently treat the muscovite closure isotherm as horizontal. We ignore errors introduced by this assumption because they generate a maximum error on a surface age of $< 0.15 \text{ Myr}$, equalling $\sim 25\%$ of the average analytical error on the muscovite cooling ages in this study.

Temporal response

In general, the model predicts that $\sim 20 \text{ Myr}$ are required to attain a thermal steady state under a constant erosion regime. With a fixed topographic relief of 4 km, we investigated the temporal response of the 350° C isotherm to changes in erosion rate for two scenarios: an instantaneous change in rate from 0 to some fixed rate and an instantaneous change from one fixed rate to another. The results show two clear trends: thermal equilibrium is attained

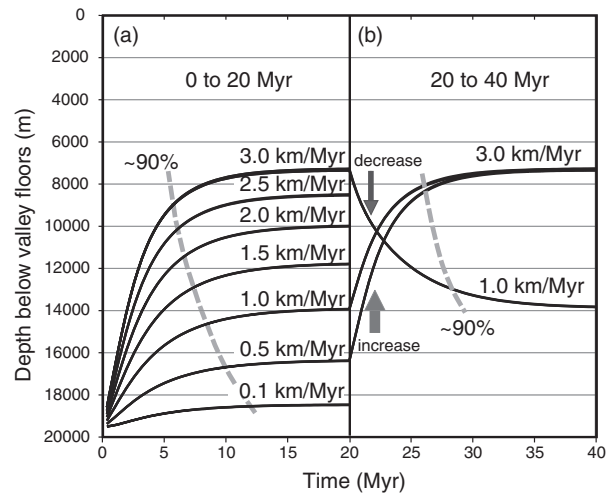


Fig. 1. Temporal response of the depth of the 350° C isotherm for a system with 4 km of topographic relief. (a) Starting from a thermal steady state in the absence of topography and erosion, temporal changes in the depth of the 350° C isotherm are depicted for uniform erosion rates of 0.1 to 3.0 km Myr^{-1} (labelled). (b) After 20 Myr, three scenarios show the response to: (i) a decrease in erosion from 3.0 to 1.0 km Myr^{-1} ; (ii) an increase in erosion from 1.0 to 3.0 km Myr^{-1} , and (iii) an increase in erosion from 0.5 to 3.0 km Myr^{-1} . Dashed lines approximate the time required to attain 90% of the equilibrium position of the closure isotherm.

more rapidly when erosion rates are higher (Fig. 1a); and equilibrium is approached more rapidly when rates are increasing, rather than decreasing (Fig. 1b). The model predicts that 5–10 Myr are required to approach to within 90% of thermal equilibrium. For intermediate temperature thermochronometers, such as muscovite, this result implies that deformation and erosion must remain steady for 5 Myr or more before a thermal steady state can be approached (Willett & Brandon, 2002). Consequently, orogens subjected to changes in tectonic rates since the early Pliocene time are unlikely to be in thermal equilibrium for $^{40}\text{Ar}/^{39}\text{Ar}$ muscovite studies, and erosion rates over this interval will be more difficult to estimate reliably. Nonetheless, because advecting rocks carry heat with them, nearly 80% of the equilibrium temperature is attained within 3–5 Myr (Fig. 1).

Modelled closure isotherm

Based on our model results and for easy integration into our detrital cooling-age model, the depth of the closure isotherm is predicted using an empirically fit equation ($r^2 = 0.98$) that incorporates an exponential increase of topographic deflection and exponentially decreasing depth of the closure isotherm with increasing erosion rate:

$$z_c = (k_1 e^{-k_2 \varepsilon} - k_3)R + k_4 e^{-k_5 \varepsilon} \quad (2)$$

where z_c is the depth of the 350° C isotherm, ε is the erosion rate, R is the relief and k_1 to k_5 are empirical constants.

Although exact interpretations of thermochronological data in specific orogens require accurate reconstruction of isotherms, our model uses a simplified topography and is only applicable for those conditions with approximately horizontal closure isotherms and with erosion rates $\leq 3 \text{ km Myr}^{-1}$ and relief $\leq 6 \text{ km}$. Most orogens fall within these limits on erosion rates and relief, but the errors introduced by our simplified topography, vertical particle trajectories, and assumed thermal equilibrium should be assessed in each orogen.

Topographic steady state

Our model also assumes that the rock uplift is balanced by erosion and that a topographic steady state prevails (Montgomery, 2001; Willett *et al.*, 2001), such that mean elevation, relief, and hypsometry are time invariant. For orogens where erosion rates are $\geq 1 \text{ km Myr}^{-1}$, numerical models predict that topographic steady state will be attained at time scales ($\sim 1 \text{ Myr}$) that are considerably shorter than the time needed to come to a thermal steady state (Kooi & Beaumont, 1996; Willett, 1999). In detail, of course, climate drives changes in erosion rates at $\sim 10^4$ -year time scales and thereby is likely to modify the average topographic characteristics of orogens. We assume that these departures represent oscillations around a mean that are equivalent to a dynamic topographic steady state (Burbank, 2002). Overall, we contend that short-term variations in relief or erosion rate should have little impact on the mean position of the 350°C isotherm with respect to the surface and that many such oscillations will be integrated and averaged during the time between crossing of the closure isotherm and erosion at the surface.

Age distributions for a theoretical catchment

River catchments within orogens provide a readily defined framework within which to consider the detrital cooling-age signal. For this model, we assume that source-area catchments are small enough to drain a single tectonic zone, such that each point in the catchment experiences the same erosion rate and shares a common thermal history for the specified relief and catchment erosion rate. To warrant use of such assumptions, large and complex catchments have to be subdivided into smaller tributary catchments with more uniform characteristics.

By combining our assumed vertical particle trajectories with depth estimates of the closure isotherm as a function of erosion rate and relief, modelled cooling ages in a catchment will increase linearly with elevation. The vertical distance from a horizontal 350°C isotherm to valley bottoms, for example, is less than the distance to mountain summits and is reflected in younger bedrock cooling ages at the base of a mountain (Fig. 2). Thus the cooling age (t_c) of a point in the landscape can be calculated from:

$$t_c = \frac{(z_x - z_c)}{dz/dt} \quad (3)$$

where z_x is the elevation of the sample location, z_c is the elevation of the closure isotherm as calculated in Eqn. (2) and dz/dt is the erosion rate. We can examine the consequences of varying the erosion rate on the predicted age range for catchments with 2, 4, and 6 km of relief (Fig. 3). As the erosion rate increases, the summits and valley floors exhibit younger cooling ages, but in addition, the range of cooling ages between valley and summits decreases as the closure isotherm becomes shallower.

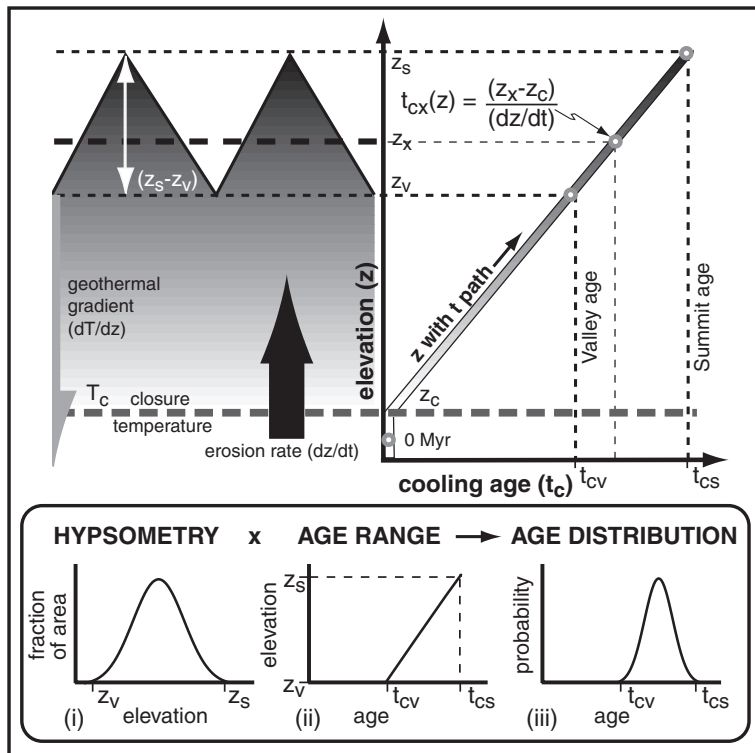


Fig. 2. Construction of a 'theoretical' distribution of ages for an individual basin. A cooling age (t_c) is calculated from the depth (z_c) of the closure temperature (T_c) for which z_c is a result of the thermal model and the erosion rate (dz/dt). The difference between summit elevation (z_s) and valley elevation (z_v) results in a difference between summit cooling ages (t_{cs}) and the valley cooling ages (t_{cv}). The cooling age (t_{cx}) of a sample 'x' derived from elevation z_x can be calculated using the equation shown. The inset illustrates how the age distribution is governed by the combination of the age range (t_{cv} to t_{cs}), and the relationship of land area to elevation (hypsometry), which is shown as a normal distribution here.

The range of cooling ages in a bedrock source area can be calculated by combining Eqs (2) and (3) with a specified erosion rate and topographic relief. The relative frequency (considered as a probability density function: PDF) of any age within that range, as sampled in the basin, is calculated by multiplying the source-area hypsometry (a PDF of altitude as extracted from digital elevation model) by the age–altitude relationship (Fig. 2). If there is no storage of sediment within the catchment, the theoretical PDF of detrital cooling ages at the basin mouth will exactly reproduce the PDF of bedrock cooling ages in the source area.

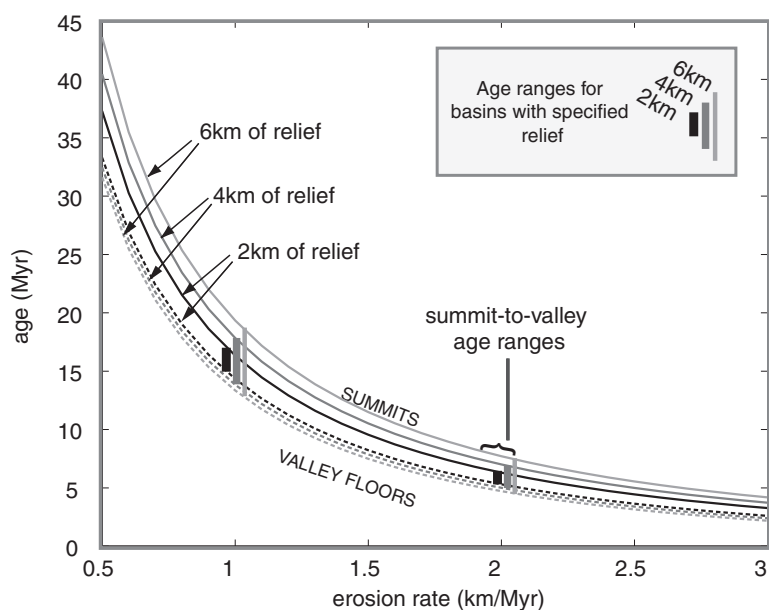
Three assumptions are embedded in this modelling approach: (1) uniform erosion rates across the catchment; (2) homogeneous distribution of the mineral being dated and (3) insignificant transport and storage times within the system. To the extent that the rock uplift rate is spatially constant, uniform erosion rates are a necessary consequence of the assumed topographic steady state. If appropriately sized source-area catchments are chosen, spatial variations in rock uplift should commonly be small, and valley bottoms and ridge crests should be lowered at the same rate (Burbank *et al.*, 1996; Montgomery & Brandon, 2002). Whether or not a homogeneous distribution of the target mineral to be dated exists within a source-area catchment is often unknown. In actuality, the detrital cooling-age PDF will be weighted towards lithologies that supply more thermochronometer per unit area. If the source-area catchment is chosen such that a single lithostratigraphic unit occurs within it, a homogeneous distribution is more likely than if several contrasting rock units transect the catchment. If a given lithology is known to be devoid of the target mineral, areas underlain by this lithology can be excluded from the catchment hypsometry. For example, limestone commonly contains little muscovite, so that, for detrital dating studies based on muscovite, the hypsometry of terrain underlain by carbonates could be subtracted from the overall source-area hypsometry.

The assumption of insignificant sediment storage can be validated for most catchments in actively eroding orogens. If erosion rates are $\geq 0.5 \text{ mm yr}^{-1}$, landslides dominate nonglacial hillslopes and rivers must flow across the bedrock in order to incise. Neither process permits significant long-term storage within the catchment. At much lower erosion rates, such as 0.1 mm/yr , even if sediment were to be stored for 1 Myr, this storage would represent a small fraction of the integrated time since passage through the closure temperature and would, therefore, introduce minimal errors.

RELIEF AND EROSION CONTROLS ON A THEORETICAL PDF

The PDF of ages emerging from a catchment is theoretically predictable based on relief, erosion rate, and hypsometry. If we assume a Gaussian-distributed hypsometry for a modelled catchment, the trade-offs between relief and erosion rate are reflected in age PDFs (Fig. 4). Increasing the relief of a catchment broadens the span of ages in the PDF as the vertical separation between the summit and closure isotherm increases. Increasing erosion rate generates younger ages and narrows the width of the PDF for a given catchment relief (Figs 3 and 4). These relations suggest that, on the basis of an observed distribution of detrital ages, we have the potential to invert the relief and erosion rate from the geological record, as suggested for palaeorelief by Stock & Montgomery (1996). With an appropriate record of detrital cooling ages from foreland basin sediments, we could in theory test the hypothesis of Molnar & England (1990) that increased Quaternary incision drove relief production or that increased runoff decreases relief (Whipple *et al.*, 1999). If both relief and erosion rates increased in Quaternary times (Molnar & England, 1990; Zhang *et al.*, 2001), we would expect the

Fig. 3. Relationship between summit ages (solid lines) and valley ages (dashed lines) for topographic relief of 2, 4, and 6 km undergoing erosion rates of 0.5 to 3.0 km Myr⁻¹. The vertical bars illustrate the age range with elevation for erosion rates of 1.0 and 2.0 km Myr⁻¹. The range in ages is a function of erosion rate and the relief. The range narrows as the erosion rate increases, and 2 km of relief (black lines) contains a smaller range of ages than 4 km of relief (dark grey lines), which in turn is smaller than 6 km of relief (light grey lines).



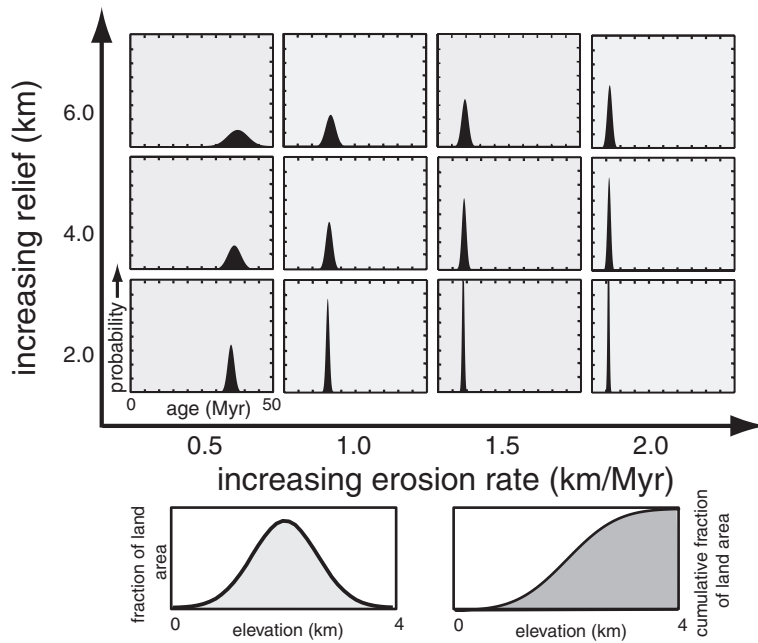


Fig. 4. Effects of uplift rate and relief on theoretical PDFs for a basin with a Gaussian distribution of land area with elevation (illustrated in the bottom two plots). In the calculations, the depth to the 350 °C isotherm is taken from our thermal modelling. The scale of each inset theoretical-PDF plot is the same with the x-axis ranging from 0 to 50 Myr, and probability on the y-axis.

detrital PDFs from Himalayan basins to move diagonally up and to the right in Fig. 4, displaying a younger mean age with the range in ages dependent on the change in relief.

To explore the effects of hypsometry, we examine idealized end-member basin morphologies: hypsometries where most of the catchment is situated in the top, base, or middle of the catchment relief (Fig. 5). If land area is concentrated in lower elevations, such as would occur in a piedmont with isolated inselbergs, the cooling-age signal will be biased towards young ages (Fig. 5, case a). If a catchment includes a high plateau, older ages will predominate (Fig. 5, case e). Basins with land concentrated in the middle reaches (Fig. 5, case d) display normally distributed cooling-age PDFs like those modelled in Fig. 1. These could typify steep fluvial basins, but glacial erosion also appears to concentrate alpine topography towards the middle elevations of basins with very high relief (Brozović *et al.*, 1997).

APPLICATION TO TWO HIMALAYAN BASINS

Geological setting of the sample sites

To illustrate the modelling method outlined above, we consider ⁴⁰Ar/³⁹Ar detrital muscovite data for Nepalese sediment samples from the Marsyandi River and one of its tributaries, the Dordi Khola (Fig. 6). Along its course, the Marsyandi transects many of the tectonostratigraphic zones of the Himalayan-Tibetan orogen (see Hodges, 2000 for review). Its headwaters lie within weakly metamorphosed to unmetamorphosed Indian passive margin (Tethyan) strata of the Tibetan zone. After crossing the Machhapuchhare Detachment Fault, the Chame Detachment fault (the basal structure of the South Tibetan fault

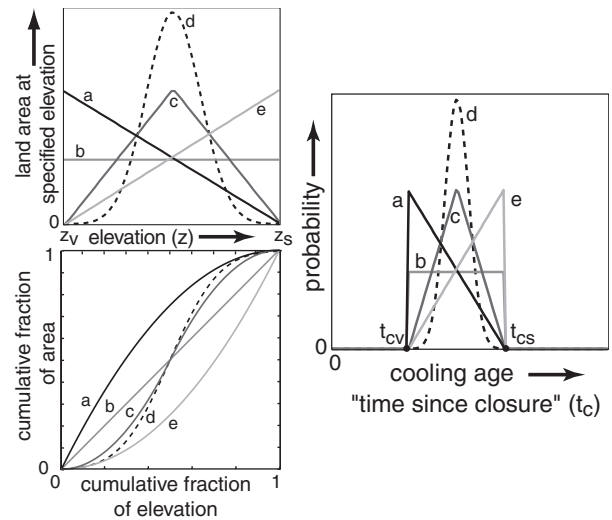


Fig. 5. Effects of hypsometry on theoretical PDFs. The upper left panel shows the relationship between a specific elevation and the land area at that elevation for five basins. The cumulative hypsometric curves are shown in the lower left panel. The right panel shows the resulting theoretical PDF for the basin. The range in ages (t_{cv} to t_{cs}) is dependent upon the specified erosion rate. Basin (a) contains most land at lower elevations, whereas (e) contains most land at higher elevations. Basin (b) has a uniform distribution of land with elevation, and (c) is biased towards concentration in the middle elevations. Basin (d) has a normal distribution of land with elevation that was used as an approximation in the sensitivity analyses (Fig. 4).

system in this area (Coleman, 1996)), the Marsyandi enters the Annapurna and Manaslu massifs, where high-grade metasedimentary and meta-igneous rocks of the Greater Himalayan zone have been intruded by Oligo-Miocene leucogranites. Finally, as the river passes through the Himalayan foothills, its bedrock includes deformed

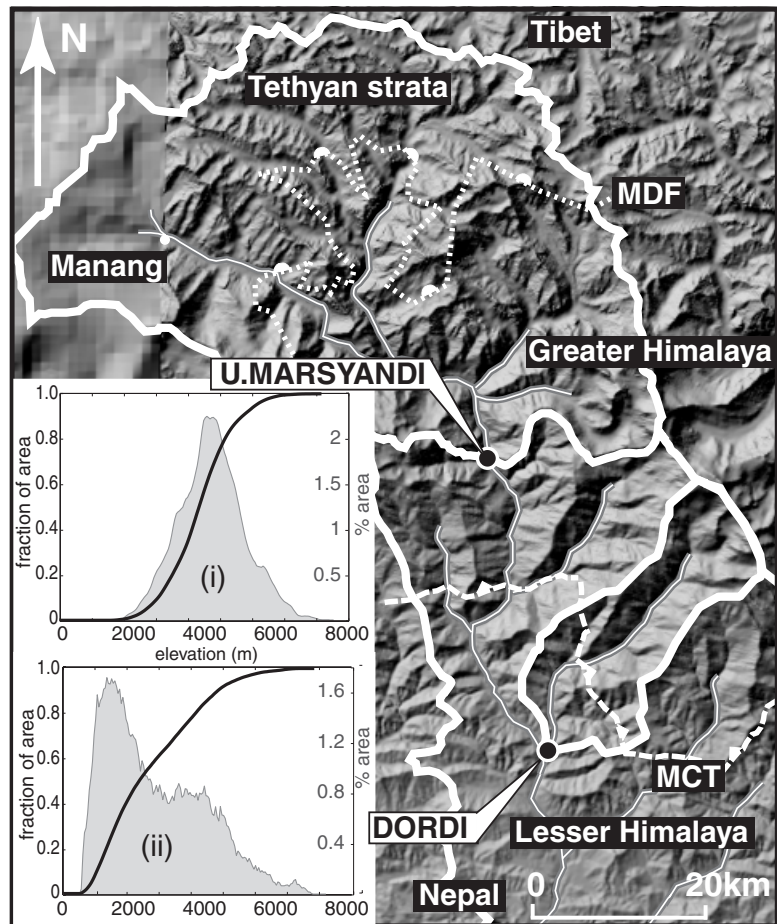
metamorphic rocks of the Main Central Thrust (MCT) zone and footwall metasedimentary rocks of the Lesser Himalayan zone. The MCT and the detachment faults at the base of the Tethyan rocks have been interpreted to have been synchronously active between 16 and 20 Ma (Burchfiel *et al.*, 1992; Hodges, 2000).

Sample 1 comprises modern riverbed sediments of the Marsyandi ~ 40 km downstream from the trace of the Machhapuchhare detachment (Fig. 6). Potential source regions for the muscovite in this sample include the structurally highest Greater Himalayan gneisses and leucogranites (which yield $^{40}\text{Ar}/^{39}\text{Ar}$ muscovite plateau dates of ~ 17 – 18 Ma in this area (Coleman & Hodges, 1995; Copeland *et al.*, 1990)) and rare hydrothermal veins in Tibetan zone sedimentary rocks (with $^{40}\text{Ar}/^{39}\text{Ar}$ muscovite plateau dates of ~ 14 Ma (Coleman & Hodges, 1995)). Sample 2 was collected in the Dordi Khola, ~ 400 m upstream of its confluence with the Marsyandi. This catchment includes the structurally middle and lower parts of the Greater Himalayan zone, the MCT zone, and the uppermost Lesser Himalayan zone rocks. Although few bedrock $^{40}\text{Ar}/^{39}\text{Ar}$ muscovite data are available for the middle and lower Greater Himalayan rocks in the Marsyandi drainage area, samples from equivalent structural levels in the Kali Gandaki drainage (~ 80 km to the west) yield ~ 15 Ma $^{40}\text{Ar}/^{39}\text{Ar}$ dates (Vannay & Hodges, 1996). Muscovite dates

of 6.2 ± 0.2 and 2.6 ± 0.1 Ma from the MCT zone in the Marsyandi valley (Edwards, 1995) suggest that Sample 2, which includes this zone, should yield considerably younger $^{40}\text{Ar}/^{39}\text{Ar}$ dates. Such young cooling ages support other thermochronological evidence for widespread Late Miocene–Pliocene erosion and cooling of the MCT zone and its footwall in the central Nepalese Himalaya (Copeland *et al.*, 1991; MacFarlane *et al.*, 1992; Macfarlane, 1993; Harrison *et al.*, 1997; Catlos *et al.*, 2001; Robinson *et al.*, 2001, 2003).

Based on data extracted from a 90-m digital elevation model, the upper Marsyandi basin (Fig. 6(i)) contains 6500 m of relief within its 2270 km², of which 1230 km² comprises Tethyan sediments according to the map of Colchen *et al.* (1986). We consider only the remaining 1140 km² of the basin that drains the top of the Greater Himalaya sequence, because, as indicated by point counting, the rare hydrothermal muscovites, as well as the Tethyan carbonate and mudstone strata in the Tibetan zone, make a negligible contribution to the detrital muscovite signal. According to our theoretical models, omission of this zone should not affect the range in ages of the basin because the maximum basin relief is contained within the Greater Himalaya. The hypsometry changes, however, and mean relief decreases from 4800 to 4400 m. In addition, by limiting the analysis to the area south of the Machhapuchhare Detachment

Fig. 6. Map of the upper Marsyandi drainage basin showing the detrital sample locations (black markers). The thick white lines represent the catchment areas upstream of the sample sites within the larger Marsyandi Basin. The Machhapuchhare Detachment fault (MDF) is shown with fine dashes, and the Main Central Thrust (MCT) is shown with longer dashes. The insets depict the hypsometry for (i) the upper Marsyandi (Sample 1) and (ii) the Dordi (Sample 2). The hypsometry is calculated using 50-m elevation bins, and then smoothed over 5 bins. Elevation data for the upper Marsyandi are taken from the area south of the MDF because the area to the north is composed of Tethyan sediments.



Fault, the assumption of uniform erosion rate is more likely to be valid. The Dordi Khola drains the southern front of the Himalayan topographic axis and is 351 km² in extent, with 7200 m of relief and an average elevation of 2900 m (Fig. 6(ii)).

Detrital ⁴⁰Ar/³⁹Ar cooling-age results and modelling theoretical PDFs

Individual muscovite grains between 500 and 2000 µm were analysed at the ⁴⁰Ar/³⁹Ar laser microprobe facility at the Massachusetts Institute of Technology (Hodges, 1998). In the rapidly eroding Himalayan setting, this coarse sand size provides grains with enough radiogenic ⁴⁰Ar for reliable analysis. Apparent ages (dates) calculated for each muscovite are reported in Table 1 with an estimated 2σ uncertainty obtained by propagating all analytical uncertainties. (In order to illustrate the proportion of this uncertainty that is attributable to uncertainties in the neutron flux during sample irradiation, Table 1 shows uncertainties in apparent ages calculated with and without the contribution from the irradiation parameter J). Further details on analytical techniques may be found in Hodges and Bowring (1995).

Given a date and an analytical uncertainty for that date, a probability density function can be calculated for each grain assuming that a Gaussian kernel represents the distribution of error (Bevington & Robinson, 1992; Brandon, 1996). For a sample of N grains collected from a specific locality, the PDF of the age of each dated grain can be combined to yield a summed probability density function that represents the distribution of age probability within the sample.

The ⁴⁰Ar/³⁹Ar results display distinctly different detrital signals originating from each catchment area (Fig. 7). The summed PDF for 35 grains for the upper Marsyandi basin spans ages from 11.2 ± 1.4 to 18.7 ± 1.3 Myr and is characterized by a sharp peak at ~17 Myr and a 'tail' of younger grains from 10 to 14 Myr. The peak is comparable to bedrock muscovite ⁴⁰Ar/³⁹Ar ages from the upper Greater Himalaya sequence (Copeland *et al.*, 1990; Coleman & Hodges, 1995). The Dordi Khola contains 39 grains that range from 2.6 ± 1.2 to 12.7 ± 0.5 Myr. The summed PDF is characterized by multiple peaks between 3 and 8 Myr, and a single peak at ~13 Myr.

We can now model these results. Given the measured hypsometry for the sampled basins, our model predicts the forms of PDFs that would be expected to be observed for a given vertical erosion rate under steady-state conditions. Recall that steady-state topography requires that the hypsometry remains nearly constant through time. Thus, by varying the erosion rate, we can match the predicted curve to the observed summed PDF and determine the solution that results in the lowest mismatch (as defined below). With this methodology, we estimate the approximate erosion rate for the upper Marsyandi basin (Sample 1) as 0.95 km Myr⁻¹ and for the Dordi Khola basin (Sample 2) as 2.15 km Myr⁻¹ (Fig. 7). Although the distribution of

ages within the two samples is about what we would expect if the erosion rates were a factor of two higher in the Dordi Khola basin than the upper Marsyandi basin (cf. Figs 3 and 4), our ability to reproduce the simple summed PDF of Sample 1 is much greater than our ability to match the more complex function of Sample 2.

Assessment of model and data mismatches

The mismatch of observed versus predicted data for Sample 2 would be expected if the riverbed sediments failed to represent the distribution of bedrock cooling ages in the Dordi Khola. Additional detrital and bedrock age determinations could test this possibility. Such a mismatch could also occur if one or more of the initial model assumptions were incorrect. For example, if the MCT zone has been reactivated during the latest Miocene or Pliocene (MacFarlane *et al.*, 1992; Harrison *et al.*, 1997; Robinson *et al.*, 2001), the assumptions of uniform uplift rates and steady-state behaviour may be erroneous. Under such circumstances, the pattern of bedrock cooling ages through the MCT zone might reflect local complexities in thermal structure and not the simple, depth-dependent distribution of isotherms required by our modelling scheme. Better resolution of the bedrock cooling-age distribution would help test this hypothesis. Alternatively, the relatively small number of grains analysed at each locality might be insufficient to characterize the true population of detrital muscovite ages adequately. Given the fact that any reasonable detrital mineral thermochronological study involves a random sampling of only a tiny fraction of the total muscovite grains at a particular site, how confident can we be that such a sample is representative? We focus on this problem in our subsequent analysis to explore the fidelity with which random picks of grains (which we define as a 'grab sample') from a synthetic population reproduce the population PDF as a function of the number of grains in the sample.

To simulate the random dating of grains from a grab sample containing millions of particles, Monte Carlo integration (Press *et al.*, 1992) is performed on the theoretical PDF (see Fig. 7). Using the MATLAB random number generator, a number of 'grains' equivalent to the number of dated grains in the sample are chosen at random from the theoretical PDF. To construct a synthetic summed PDF for each Monte Carlo age pick, a standard deviation for the apparent age of the pick has to be specified. For this model, we use a standard deviation of 0.64 Myr, which is equivalent to the average observed standard deviation of the dated grains (Table 1).

Given a grab-sample summed PDF, we need to assess the match between it and the theoretical PDF. In particular, with a finite number of grains (20–100), how well can we expect to reproduce the characteristics of the theoretical PDF? To quantify the match (or mismatch), we compute the sum of the difference in the distribution of probability (P_{diff}) between the theoretical probability ($P_{\text{theoretical}}$) and grab-sample probability (P_{grab}) over each age increment

Table 1. $^{40}\text{Ar}/^{39}\text{Ar}$ dates.

Sample	$^{36}\text{Ar}/^{40}\text{Ar} (\times 10^{-4})$	$^{39}\text{Ar}/^{40}\text{Ar} (\times 10^{-1})$	$^{39}\text{Ar} (\times 10^{-14})$ mol)*	$^{40}\text{Ar}^*$ (%)†	Age (Myr)‡ (with f)	(w/o f)
NIB-S8-1	1.17 ± 0.18	3.38 ± 0.19	10.033	96.4	18.41 ± 1.09	1.07
NIB-S8-2	2.65 ± 0.34	3.3 ± 0.12	5.779	92	18.03 ± 0.77	0.74
NIB-S8-3	3.63 ± 0.86	3.45 ± 0.42	11.365	89.1	16.71 ± 2.31	2.3
NIB-S8-4	1.45 ± 0.17	3.51 ± 0.19	10.69	95.5	17.59 ± 1.02	1
NIB-S8-5	1.49 ± 0.21	3.28 ± 0.21	7.991	95.4	18.77 ± 1.27	1.25
NIB-S8-6	4.02 ± 0.35	3.28 ± 0.21	6.238	88	17.34 ± 1.25	1.24
NIB-S8-7	0.92 ± 0.23	3.56 ± 0.14	10.337	97.1	17.62 ± 0.73	0.71
NIB-S8-8	1.02 ± 0.2	3.36 ± 0.19	8.765	96.8	18.61 ± 1.1	1.08
NIB-S8-9	2.46 ± 0.54	3.45 ± 0.13	3.931	92.6	17.33 ± 0.77	0.74
NIB-S8-10	1.15 ± 0.4	3.65 ± 0.13	6.942	96.4	17.09 ± 0.69	0.66
NIB-S8-11	2.63 ± 0.45	3.71 ± 0.3	11.485	92.1	16.05 ± 1.45	1.43
NIB-S8-12	1.5 ± 0.25	3.48 ± 0.19	9.587	95.4	17.7 ± 1.04	1.02
NIB-S8-13	2.45 ± 0.25	3.6 ± 0.19	6.635	92.6	16.61 ± 0.97	0.95
NIB-S8-14	2.01 ± 0.31	3.47 ± 0.16	9.348	93.9	17.49 ± 0.87	0.85
NIB-S8-15	2.43 ± 0.33	3.62 ± 0.16	8.191	92.7	16.55 ± 0.83	0.81
NIB-S8-16	1.14 ± 0.24	3.44 ± 0.19	6.462	96.5	18.1 ± 1.07	1.05
NIB-S8-17	2.17 ± 0.33	3.8 ± 0.1	7.448	93.4	15.89 ± 0.5	0.47
NIB-S8-18	2 ± 0.32	3.66 ± 0.24	8.758	93.9	16.6 ± 1.17	1.16
NIB-S8-19	1.47 ± 0.2	3.54 ± 0.1	8.72	95.5	17.43 ± 0.57	0.53
NIB-S8-20	1.21 ± 0.44	3.69 ± 0.18	4.093	96.2	16.85 ± 0.89	0.86
NIB-S8-21	3.26 ± 5.52	3.7 ± 0.19	4.293	90.2	15.75 ± 2.98	2.97
NIB-S8-22	4.74 ± 3.66	3.3 ± 0.09	5.93	85.9	16.83 ± 2.18	2.17
NIB-S8-23	6.38 ± 2.31	3.04 ± 0.06	8.623	81	17.22 ± 1.52	1.5
NIB-S8-24	3.64 ± 2.89	3.49 ± 0.12	7.674	89.1	16.5 ± 1.71	1.7
NIB-S8-25	3.92 ± 5.78	3.56 ± 0.18	3.919	88.3	16.02 ± 3.22	3.22
NIB-S8-26	3.39 ± 3.67	5.21 ± 0.22	9.067	89.7	11.17 ± 1.44	1.44
NIB-S8-27	2.79 ± 4.35	3.45 ± 0.16	5.056	91.6	17.18 ± 2.56	2.55
NIB-S8-28	2.64 ± 3.26	3.87 ± 0.17	7.795	92	15.38 ± 1.77	1.76
NIB-S8-29	4.78 ± 6.51	3.54 ± 0.23	3.483	85.7	15.68 ± 3.69	3.69
NIB-S8-30	1.73 ± 2.41	3.39 ± 0.06	8.984	94.7	18.07 ± 1.41	1.4
NIB-S8-31	3.59 ± 3.03	3.26 ± 0.12	6.868	89.2	17.69 ± 1.92	1.91
NIB-S8-32	3.87 ± 4.93	3.4 ± 0.14	4.397	88.4	16.81 ± 2.87	2.86
NIB-S8-33	2.64 ± 4.76	3.26 ± 0.15	4.39	92.1	18.26 ± 2.93	2.93
NIB-S8-34	5.72 ± 7.7	3.22 ± 0.17	2.789	83	16.65 ± 4.65	4.65
NIB-S8-35	2.4 ± 4.26	3.6 ± 0.12	5.358	92.8	16.64 ± 2.33	2.32
NIB-S44-1	1.74 ± 14.36	8.16 ± 0.74	0.552	94.5	7.05 ± 3.23	3.22
NIB-S44-2	9.02 ± 6.28	8.44 ± 0.17	1.182	73	5.27 ± 1.35	1.34
NIB-S44-3	5.7 ± 2.77	8.94 ± 0.2	2.596	82.8	5.65 ± 0.59	0.57
NIB-S44-4	6.35 ± 10.74	12.13 ± 1.03	0.983	80.7	4.07 ± 1.65	1.64
NIB-S44-5	4.55 ± 8.99	7.63 ± 0.09	1.511	86.2	6.88 ± 2.12	2.11
NIB-S44-7	3.08 ± 2.17	7.96 ± 0.66	5.565	90.5	6.93 ± 0.82	0.8
NIB-S44-8	1.43 ± 4.54	8.07 ± 0.22	1.949	95.4	7.2 ± 1.04	1.03
NIB-S44-9	6.32 ± 8.48	9.3 ± 0.16	1.411	81	5.31 ± 1.64	1.64
NIB-S44-10	4.18 ± 3.86	7.26 ± 0.55	3.541	87.3	7.32 ± 1.15	1.14
NIB-S44-11	4.76 ± 3.33	8.03 ± 0.67	3.733	85.6	6.49 ± 0.99	0.97
NIB-S44-12	2.46 ± 4.3	10.88 ± 0.88	3.519	92.2	5.17 ± 0.85	0.84
NIB-S44-13	7.77 ± 4.77	8.36 ± 0.4	2.022	76.7	5.59 ± 1.08	1.07
NIB-S44-14	4.06 ± 4.67	8.27 ± 0.19	1.558	87.6	6.46 ± 1.04	1.03
NIB-S44-15	5.56 ± 6.26	5.63 ± 0.16	1.124	83.3	9 ± 2.02	2.01
NIB-S44-16	2.01 ± 4.11	9.45 ± 0.74	2.723	93.6	6.04 ± 0.94	0.93
NIB-S44-17	8.21 ± 2.53	10.94 ± 0.43	7.538	75.3	4.21 ± 0.48	0.47
NIB-S44-18	11.48 ± 3.59	9.16 ± 0.75	3.287	65.8	4.38 ± 0.87	0.87
NIB-S44-19	5.73 ± 7.72	7.42 ± 0.41	1.154	82.7	6.79 ± 1.92	1.91
NIB-S44-20	20.07 ± 22.18	8.97 ± 0.71	0.472	40.5	2.76 ± 4.46	4.46
NIB-S44-21	1.83 ± 4.6	11.09 ± 0.31	1.321	94.1	5.18 ± 0.77	0.76
NIB-S44-22	4.86 ± 2.46	10.44 ± 0.14	2.003	85.2	4.98 ± 0.45	0.43
NIB-S44-23	6.61 ± 0.75	8.25 ± 0.23	6.18	80.1	5.92 ± 0.3	0.26
NIB-S44-24	6.87 ± 0.71	7.43 ± 0.07	6.169	79.4	6.51 ± 0.25	0.19

Table 1. (Contd.)

Sample	$^{36}\text{Ar}/^{40}\text{Ar} (\times 10^{-4})$	$^{39}\text{Ar}/^{40}\text{Ar} (\times 10^{-1})$	$^{39}\text{Ar} (\times 10^{-14})$ mol)*	$^{40}\text{Ar}_*$ (%)†	Age (Myr)‡ (with \mathcal{J})	(w/o \mathcal{J})
NIB-S44-25	7.21 ± 0.63	8.66 ± 0.13	9.533	78.4	5.52 ± 0.22	0.17
NIB-S44-26	3.59 ± 0.64	4.25 ± 0.07	2.929	89.2	12.75 ± 0.48	0.36
NIB-S44-27	13.28 ± 2.94	9.05 ± 0.33	2.153	60.5	4.08 ± 0.63	0.62
NIB-S44-28	11.42 ± 2.98	12.85 ± 0.64	2.068	65.8	3.13 ± 0.48	0.47
NIB-S44-29	7.19 ± 1.02	8.24 ± 0.12	3.437	78.4	5.8 ± 0.29	0.25
NIB-S44-30	16.81 ± 1.03	7.14 ± 0.08	3.75	50.1	4.28 ± 0.29	0.27
NIB-S44-31	9.55 ± 0.76	7.93 ± 0.1	5.262	71.5	5.5 ± 0.24	0.19
NIB-S44-32	10.26 ± 2.84	10.67 ± 0.55	2.772	69.3	3.97 ± 0.56	0.55
NIB-S44-33	6.75 ± 1.52	8.33 ± 0.15	3.728	79.7	5.83 ± 0.38	0.35
NIB-S44-34	14.96 ± 3.07	8.28 ± 0.16	1.35	55.6	4.09 ± 0.69	0.68
NIB-S44-35	13.45 ± 1.19	6.32 ± 0.09	3.469	60.1	5.79 ± 0.39	0.36
NIB-S44-36	6.4 ± 0.94	6.98 ± 0.02	5.453	80.8	7.05 ± 0.3	0.24
NIB-S44-37	12.78 ± 2.62	8.38 ± 0.21	1.638	62	4.51 ± 0.6	0.59
NIB-S44-38	23.05 ± 4.96	7.59 ± 0.29	0.988	31.8	2.55 ± 1.19	1.19
NIB-S44-39	11.74 ± 0.7	6.92 ± 0.03	4.474	65.1	5.73 ± 0.23	0.18
NIB-S44-40	22.83 ± 2.17	4.6 ± 0.18	1.217	32.5	4.29 ± 0.93	0.93
Total samples: 74				Mean error	0.64	
				1σ on error	0.49	

Assigned uncertainty corresponds to 2σ error.

*Number of moles of K-derived ^{39}Ar ($^{39}\text{Ar}_K$) released during fusion.

†Percentage of radiogenic ^{40}Ar ($^{40}\text{Ar}_*$) in the total ^{40}Ar for each analysis.

‡Age uncertainties are shown with and without propagated error in the irradiation parameter \mathcal{J} . Sample NIB-S8 corresponds to Sample 1 in the text, and sample NIB-S44 corresponds to Sample 2. Grain 6 in sample NIB-S44 underwent incomplete fusion and is not listed.

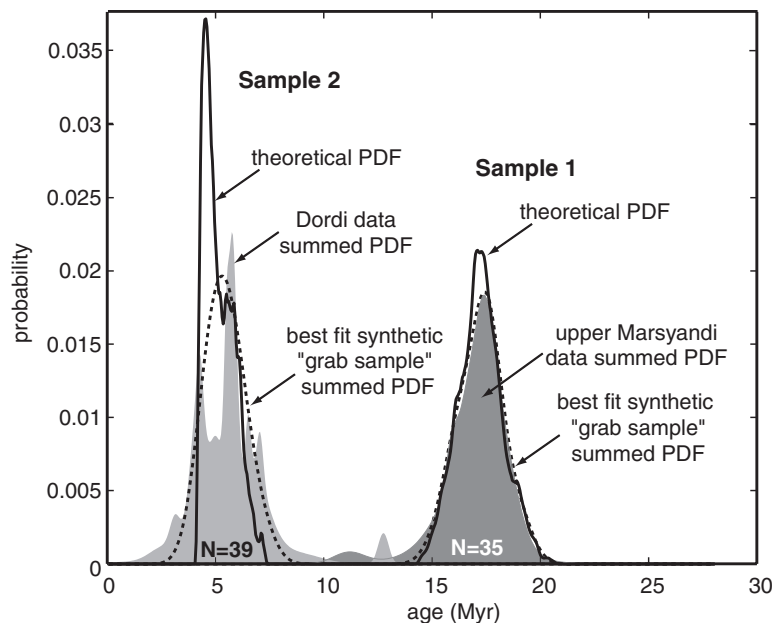


Fig. 7. Diagram showing summed PDFs generated from the results of $^{40}\text{Ar}/^{39}\text{Ar}$ dating samples from the upper Marsyandi (Sample 1) and Dordi basin (Sample 2). The black lines indicate the theoretical PDFs generated by the model for each basin. The dashed grey lines indicate the best-fit grab-sample summed PDFs (to the data) from 30 iterations. The number of grains dated (N) varies for each sample, and this determines the number of Monte Carlo picks used for generating each grab-sample summed PDF.

(t), and express this difference in terms of a percentage of total probability:

$$P_{\text{diff}} = \frac{\sum_{t=0}^{t=\infty} |P_{\text{theoretical}}(t) - P_{\text{grab}}(t)|}{2} \times 100. \quad (4)$$

This provides the percentage mismatch of the entire probability signal in the units of percentage probability

(Fig. 8). For illustration, if the two PDF curves are identical, then the error is zero percent, whereas for an error of 100%, the two curves would have completely different age ranges with no overlap in probability–age space. To investigate the range of summed PDFs that a single theoretical PDF can generate, successive iterations produce many individual synthetic ‘grab-sample’ curves for a given number of grains. The 95% confidence interval of the errors repre-

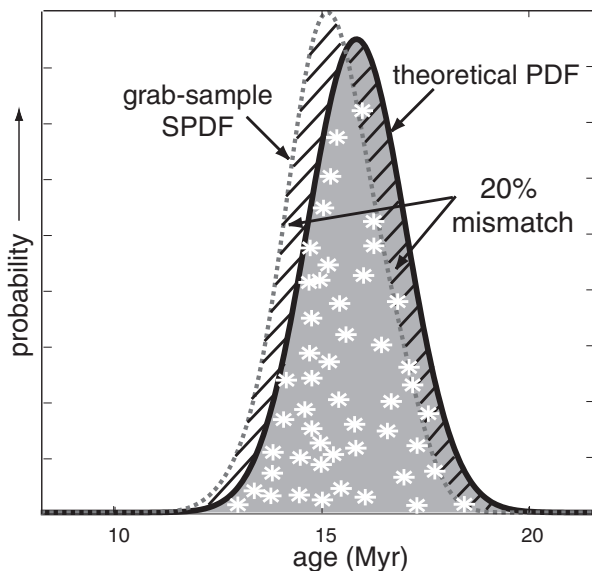


Fig. 8. Error calculation for a basin of 4-km relief eroding at 1 km Myr^{-1} , in conjunction with a normal distribution of land area with elevation. The theoretical PDF is outlined in black and shaded, whereas the grab-sample summed PDF, containing 50 grains, is outlined by the grey dashed line. The white stars are a cartoon illustration of the Monte Carlo sampling of grains from the theoretical PDF (note that they all fall inside the black curve). The x -axis values of the stars are used as the reported mean age and, with a specified error, are used to produce Gaussian-distributed kernels for each grain. The grab-sample-summed PDF is the summation of the individual grain kernels normalized to unity. The area with diagonal hatching represents the total mismatch between the theoretical PDF and the grab-sample summed PDF, which is 40% of the total probability (area) of the theoretical PDF, or an error of 20%.

sending all iterations is taken as the measure of how well the specified number of grains represents the theoretical PDF.

Before examining the observed data, we assess the resolution of the detrital dating methodology to determine (i) how small a change in an age distribution can be detected using a given number of dates and (ii) how statistically similar or different are observed or synthetic detrital age distributions. Initially, we address the problem of whether summed PDF 'A' can be explained by the statistical variability of 'B' due to random grain selection. For this test, we generate a theoretical curve that best matches B. Numerous model iterations (with the number of grains in each iteration equal to that contained in A) serve to define the most likely range of outcomes. If the misfit between A and B is less than the $2\text{-}\sigma$ error on the range of modelled outcomes, A and B are statistically indistinguishable at the 95% confidence level.

To investigate how well different numbers of grains match the theoretical sample, we consider a basin with 4 km of relief eroding at 1.0 km Myr^{-1} (Fig. 9, scenario a). For each specified number of grains, 1000 iterations define the 95% confidence limits on the error related to the mismatch of theoretical and 'grab-sample' PDFs. As

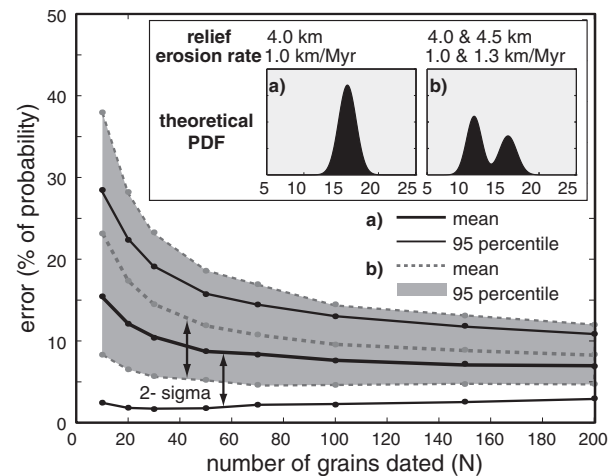


Fig. 9. Number of grains vs. the mismatch error from 1000 iterations. The mean is shown with thick lines and the 95% confidence envelope is shown with thinner lines. Two scenarios are illustrated: (a) a theoretical PDF from a single basin with 4 km of relief eroding at 1 km Myr^{-1} (solid black line as mean) and (b) a more complex theoretical PDF constructed from a basin with 4.0 km of relief eroding at 1 km Myr^{-1} and a basin with 4.5 km of relief eroding at 1.3 km Myr^{-1} (dashed grey line as mean). Note that it is harder to match the more complex theoretical PDF than the individual basin.

expected, increasing the number of grains (i) decreases the average mismatch of the grab-sample summed PDFs with respect to the real PDF and (ii) leads to more certainty in the result as the width of the 95% confidence window decreases. The initially rapid reduction in mismatch with increasing numbers of grains emphasizes the improvement accruing from additional analyses. The rate of improvement declines rapidly, however, after ~ 50 grains: increasing the number of dated grains does a better job of constraining the theoretical cooling-age signal, but with diminishing returns. With expensive dating techniques, a trade-off clearly exists between the cost of dating and the extra confidence provided by large numbers of grains.

In a drainage system, as different source areas with contrasting hypsometries, relief, and rates of erosion are blended together, the predicted age signal becomes more complex. Consider, for example, the effect of combining a catchment of 4.0-km relief eroding at 1.0 km Myr^{-1} and a basin of 4.5-km relief eroding at 1.3 km Myr^{-1} (Fig. 9, scenario b). The more complex two-basin PDF (see figure insert) is more difficult to match than the simple one-basin PDF. For any given number of dated grains, the mean mismatch of the summed PDFs is $\sim 3\text{--}8\%$ larger for the more complex PDF than for the simpler case (Fig. 9, scenario a). Overall, this statistical analysis illustrates that $\sim 60+$ grains (scenario a) and $\sim 90+$ grains (scenario b) are needed to achieve a mismatch of $\leq 15\%$ at the 95% confidence level. Although such a mismatch may seem large, much of the error comes from mismatches of the tails of the distributions (Fig. 10). Moreover, mismatches of this magnitude typify the mismatches between component

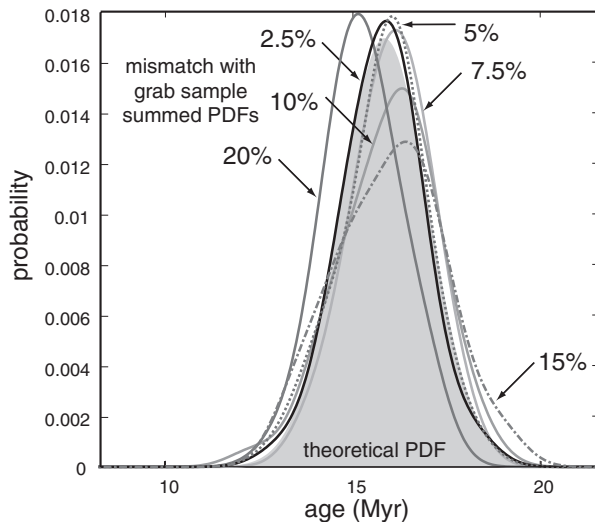


Fig. 10. A selected range of outcomes from sampling 50 grains from the theoretical PDF (shaded grey) of a basin with 4 km of relief eroding at 1.0 km Myr^{-1} (as in Fig. 8). Note that while mismatches up to 20% sound large, in reality the grab-sample summed PDF still captures the key attributes of the theoretical PDF: the peak-probability age of each grab-sample summed PDF varies less than $\pm 1 \text{ Myr}$ in comparison to the peak-probability age of the theoretical PDF. The mean mismatch for 1000 runs and 50 grains is $9 \pm 7\%$ (see Fig. 9) at the 95% confidence limit.

Gaussian peaks as extracted from real detrital age data and the data themselves (Bernet *et al.*, in press).

Himalayan catchments – synthesis of theoretical PDFs and random sampling

This modelling approach permits exploration of the differences between the theoretical and observed PDFs. When compared with the observed data, the upper Marsyandi theoretical PDF, as calculated using an erosion rate of 0.95 km Myr^{-1} , yields an error of 10%, whereas the Dordi theoretical PDF that is generated with an erosion rate of 2.15 km Myr^{-1} produces a mismatch error of 41%. From the theoretical PDFs of the two catchments, 30 grab samples were generated containing N age selections, where N is the number of grains actually dated in each basin. The best-fit summed PDF (dashed lines, Fig. 7) yields a mismatch of only 6% for the upper Marsyandi sample, but still has a 22% mismatch with the Dordi Khola sample, thereby illustrating the difficulty of fitting a complex PDF with relatively few dates.

In terms of strategies for dating detrital sediments, the model can exploit many iterations to quantify the 95% confidence interval that N grains produce on the theoretical versus observed mismatch. For example, a confidence interval of 4–19% was generated from the upper Marsyandi with 1000 iterations of picking 35 grains. The theoretical PDF of the upper Marsyandi fits the data summed PDF well, falls well within confidence limits, and indicates that the two curves are statistically indistinguishable. The fit is highly sensitive to the choice of the erosion rate, however,

because small shifts in the peak probability of the theoretical PDF away from the peak probability of the data summed PDF produce larger errors.

The theoretical PDF from the Dordi fits less well, falling outside of the 18–26% confidence interval, and the error is less sensitive to changes in the erosion rate. The very spiked summed PDF of the observed data is partly due to ages with low errors (e.g. $5.7 \pm 0.2 \text{ Myr}$), whereas the wide tails are caused by dates with large associated errors (e.g. $2.8 \pm 4.5 \text{ Myr}$). Given the mean 1σ error (0.64 Myr) that is used in the production of the theoretical PDF, both narrow and broad peaks in the observed data, as well as the range of ages that results from large errors on individual dates, are difficult to fit very closely.

Although the model successfully matches the peak probabilities, both samples show minor age populations that are problematic to replicate. The upper Marsyandi contains a young age population (10–14 Myr), whereas the Dordi includes a minor older age population (9–13 Myr) that the model does a poor job of representing. A likely cause of this failure is that some model assumptions are invalid within the model. Among these assumptions, that of uniform erosion rate across a catchment may be most suspect.

Differential erosion rates in the Dordi Basin would be geologically reasonable. A growing body of geomorphologic (Seeber & Gornitz, 1983; Lavé & Avouac, 2001), structural (Hodges *et al.*, 2002), and thermochronologic (MacFarlane *et al.*, 1992; Harrison *et al.*, 1997; Catlos *et al.*, 2001) data suggest that either the MCT zone has been active during the past 5–6 Myr or that subsurface deformation associated with a ramp structure on the Himalayan sole thrust has led to differential uplift across the Himalayan topographic front. To examine a basic scenario of differential erosion, the Dordi basin can be divided into two regions, in which the MCT separates the Greater Himalaya and Lesser Himalaya (see Fig. 6). For example, with erosion rates of $\sim 2.2 \text{ km Myr}^{-1}$ in the physiographically high Greater Himalaya and $\sim 1.8 \text{ km Myr}^{-1}$ in the Lesser Himalaya foothills, together with an assumption that the latter is contributing half the amount of muscovite per unit area, the mismatch may be reduced from 41% to 34%. This still falls outside the confidence interval and the very young ages are still difficult to represent, perhaps due to hydrothermal alteration in the MCT zone (Cope-land *et al.*, 1991).

Other potential sources of mismatch include sediment storage in the system or short-term imbalances in sediment supplied to the fluvial system. As discussed earlier, significant storage can be effectively discounted due to the high erosion rates. In particular, with erosion rates of 1.7 km Myr^{-1} in the Dordi, long-term sediment storage is geometrically and volumetrically untenable. Short-term imbalances in sediment supply, however, are more difficult to discount. Large landslides and debris flows (Yamanaka & Iwata, 1982) have occurred repeatedly in the Marsyandi valley and could cause an influx of grains of a specific age (i.e. perhaps causing the characteristic 6-Myr peak in the data

from the Dordi that is not seen in the theoretical curve). Given an assumed erosion rate of 2 mm yr^{-1} and typical width/depth scaling in bedrock landslides (Ohmori, 1992), a 250 m by 250 m landslide would produce a volume equivalent to an entire year's average erosion in the entire Dordi catchment. Depending on how this sediment was flushed through the system, the detrital age signal sampled at any specific time could comprise this or several point sources with very discrete and limited age distributions. At increasingly large catchment scales, the dominance of a limited suite of landslide source areas becomes less likely.

Our highly simplified thermal model is restricted to the vertical particle pathways and could introduce another source of error. In the Himalaya, erosion occurs at least in part as rocks are uplifted along structural ramps (Hodges, 2000). Such rocks can have a complex thermal history. Cooling by the underthrusting slab, accretion of underthrust material to the hanging wall, shear heating, and time all affect the thermal structure and resulting cooling history. Clearly, improving thermal and kinematic models and the subsequent calculations of the depth to the closure isotherm will produce better insights into the tectonics.

DISCUSSION

We have presented a numerical model that investigates the parameters that control the detrital cooling-age signal from an individual catchment. The model allows testing of the effects of various parameters, such as relief in a source area or rates of erosion, on thermal structure. For any given relief or erosion rate, the model initially predicts the variation of cooling ages as a function of elevation. Combining that age-elevation model with catchment hypsometry extracted from a DEM defines the predicted frequency distribution of cooling ages within a source-area catchment. The critical role played by hypsometry has not been emphasized in most previous studies of detrital dating (Stock & Montgomery, 1996; Bernet *et al.*, 2001), but is shown here to define the shape of the detrital age PDF.

The model is underpinned by a suite of assumptions, some of which can be evaluated with field data, and others which cannot. For example, our model assumes that catchments can be chosen such that erosion rates are uniform within the catchment. This is a direct consequence of an assumed topographic steady state that requires relief and mean elevation to be preserved through time. Short-term fluctuations in topography, such as would be expected due to climatic variability (Pratt *et al.*, 2002), are largely irrelevant to the steady-state assumption at the typical time scales of thermochronologic dating ($> 10^6$ years), because a cooling age will smoothly integrate these short-term variations. Long-term changes in erosion rates, such as those suggested to be associated with the onset of late Pliocene glaciation (Zhang *et al.*, 2001), however, would probably

violate the steady-state topographic assumption because relief and mean elevation would be expected to change with a step-wise change in climate (Whipple *et al.*, 1999). As long as storage of sediments is not significant within a catchment, changes in hypsometry over time will not affect the distribution of ages seen today. In contrast, changes in relief will cause changes both in the depth of the closure isotherm (Eq. (2)) and in the range of predicted ages in a catchment (Fig. 4).

The assumption of an equilibrium thermal structure and isothermal geometry implies a further assumption that the rate of tectonic forcing has been sufficiently prolonged and steady such that a thermal steady state has been achieved. Our modelling shows that, for a given perturbation in the controlling parameters, such as a change in the long-term erosion rate, it requires $\sim 5\text{--}10$ Myr for the 350°C isotherm to achieve $> 90\%$ of its total response (Fig. 1). This result suggests that, if tectonic rates are known to have changed significantly during the past 5 Ma, an evolving thermal state, rather than the assumed thermal steady state, is likely to prevail.

An orogen's thermal and kinematic structure is typically the most difficult parameter to constrain when trying to deduce erosion rates from thermochronology, especially when using the stratigraphic record. Our assumption of uniform and vertical erosion at the catchment scale is probably the greatest simplification for many orogenic systems. The lateral advection of heat and rock mass into collisional mountain belts (Beaumont *et al.*, 1994; Willett, 1999) along underlying thrust faults will, when combined with erosional and groundwater/hydrothermal processes, determine the exact pattern of bedrock cooling ages. Moreover, in the study area, Greater Himalayan rocks are truncated by the South Tibetan Detachment fault, a Miocene structure that was active between 16–20 Ma (Hodges, 2000) and which could have induced significant cooling. Whereas the observed cooling ages in the upper Marsyandi may have resulted from cooling during tectonic denudation, our approach focuses more on the interval since the mineral passed through its closure temperature and relies on an assumption of steady erosion over that interval. The difference between a short interval of rapid erosion followed by a long interval of slow erosion cannot be differentiated from steady erosion using our techniques. If, however, one knew that erosion or cooling rates had changed sometime during the time since closure, our model would be able to predict the transient state of the thermal structure.

The assumption that the target mineral for dating is uniformly distributed within a catchment can be assessed in the field through point-counting of detrital samples from sufficiently small contributing catchments. Subsequently, the contribution from different parts of a larger catchment can be adjusted using mineral abundances in detrital samples. This is a laborious procedure, however, and with few exceptions (Brown *et al.*, 1995), uniform distribution of the target mineral is assumed in other studies. The validity of such an assumption needs more thorough

testing. Analysing detrital ages from the stratigraphic record is even more difficult because the location, relief, hypsometry, and mineral distribution in the former source areas are commonly unknown.

These many caveats dictate that the numerical model must be judiciously applied to detrital mineral dating and a sampling strategy should be adopted that minimizes the impact of unvalidated assumptions. For example, sampling a catchment dominated by only one lithology will enhance the likelihood of uniform distribution of the target mineral, whereas choosing appropriately small catchments will increase the likelihood that erosion rates are uniform within the catchment.

Our examination of the statistics of sampling, the effects of increasing the number of dated grains, and the assessment of mismatches between observed and predicted or theoretical ages helps to define appropriate experimental design and dating strategies for detrital mineral studies. The modelling suggests that, except for very simple cooling-age distributions, at least detrital 30 dates are needed to begin to approximate the likely actual distribution of ages. Although many statistical methods can be used to assess mismatches, our graphical representation of errors (Figs 9 and 10) permits a rapid visual evaluation of mismatches among observed and theoretical data.

The statistical analysis (Fig. 9) shows that, even if the exact values of the error are not known when using forward modelling, the relative increase in accuracy that is attainable by dating 70 grains, rather than 30, will be significant for most age distributions, but the increase from 70 to 150 grains may not justify the extra time and expense. As a rule-of-thumb, 50–70 grains provide a modest and commonly acceptable mismatch of ~15% for a 'grab-sample' summed PDF to a theoretical PDF for a simple basin.

Given a series of detrital summed PDFs from the stratigraphic record, we can now test if they are statistically differentiable from one another. For example, if a modelled theoretical curve typically generates 5–25% error at the 95% confidence level using 40 grains, then summed PDFs generated from 40 grains in different stratigraphic horizons cannot be statistically differentiable until the mismatch errors increase above 25%. The resultant 95% confidence interval will be dependent upon the shape and complexity of the summed PDF, the analytical age error, and the number of grains dated (Fig. 9).

The theoretical PDF model can be utilized as a tool for evaluating the relative influence of parameters controlling the detrital cooling-age signal. In addition to providing a good first-order approximation for areas that have limited constraints, numerical experimentation with the theoretical PDF related to digital landscapes brings into focus those parameters and assumptions that modulate age distributions in a landscape. The $^{40}\text{Ar}/^{39}\text{Ar}$ analysis from two modern and contrasting Himalayan catchments illustrates both the potential and pitfalls of this approach. In one instance (the upper Marsyandi sample), the modelled PDF provides a reasonable fit to the observed data; in the other, it does not. In the latter case, further analysis suggests that

the mismatch is not the product of sampling bias alone, but instead indicates that one or more of our assumptions are incorrect. Nevertheless, despite modelling mismatches, we can confidently state that the average erosion rate varies significantly between the two catchments. Even if the erosion rate is not uniform across each catchment, a spatial variation of 10–20% is insignificant compared to the difference between the two catchments considering the uncertainties on the dates and random sampling. Ultimately, detrital ages are bound to provide a more complete sampling of the source area and a better approximation of the distribution of erosion rates than can be attained from isolated bedrock cooling ages that are then extrapolated to a wider region. The challenge is to develop additional techniques to reduce the uncertainties on the interpretations of suites of detrital ages.

CONCLUSIONS

Thermochronologic ages derived from detrital minerals are a direct product of the cooling and erosion history of the source area. The frequency distribution of ages, however, is also a function of the topography, mineral distribution, and geomorphology of the contributing catchment. The hypsometry of the source-area catchment is shown to be a critical control on the PDF of ages that derives from that catchment. Understanding all these controls should underpin a thorough analysis of detrital cooling ages in the modern and stratigraphic record. Because muscovite is the mineral we have targeted for dating and because muscovite's closure temperature is ~350 °C, our thermal model predicts how the interaction of topography and erosion rate controls the depth of the 350 °C closure isotherm. Increasing the erosion rate causes an exponential decrease in the isotherm depth, whereas increasing the relief compresses the isotherms beneath valley floors. Although a thermal steady state is typically assumed when interpreting cooling ages, we show that, following a step-wise change in erosion rate, 5–10 Myr are commonly required to approach within 90% of the steady-state position of 350 °C isotherm.

Considerations of cost, time, and logistics often limit the number of ages that are obtained from a detrital sample. We use Monte Carlo analysis to examine the effects of randomly selecting a few ages from the vast pool of potential ages represented by a sediment grab sample. Quantification of the mismatch between (i) the theoretical PDF of detrital ages representing the entire sample and (ii) the PDF of a few select grains from that sample illustrates the controls exerted by the complexity (or shape) of the theoretical signal, the number of grains dated, and the precision of the dating techniques. For theoretical populations of grain ages with multiple peaks, at least 50 randomly chosen, yet precise, ages are needed to define those peaks with moderate confidence.

Application of the model to real detrital age data from two Himalayan catchments shows that, for a catchment with

a single-peaked age signal, the combination of a simple erosion rate with hypsometry successfully predicts the distribution of observed ages, whereas in a more complex catchment, significant mismatches between predicted and observed ages illustrate the need for a greater understanding of the kinematic and thermal structure of an orogen in order to interpret thermochronological information accurately. By focusing on the contribution from individual catchments characterized by uniform erosion rates, our approach provides a conceptual basis for merging data from multiple tributary catchments, each with a uniform erosion rate. Additional field and theoretical studies are needed to define how individual hinterland catchments interact and combine to produce the cooling-age signals found in a downstream basin. Only then can we use detrital mineral thermochronological data to investigate the complexities of modern orogenic deformation and to unravel the detrital age signal in the stratigraphic record with confidence.

ACKNOWLEDGEMENTS

This work was supported by the National Science Foundation Grants EAR-96-27865 and EAR-98-96048. Bill Olszewski and Michael Krol provided invaluable help at the MIT laboratory. We thank Mark Brandon and Kevin Furlong for helpful discussions. Thoughtful reviews by Brandon, K. Stüwe, N. White, and H. Gibson yielded many improvements and are gratefully acknowledged.

REFERENCES

- ADAMS, C.J., BARLEY, M.E., FLETCHER, I.R. & PICKARD, A.L. (1998) Evidence from U-Pb zircon and $^{40}\text{Ar}/^{39}\text{Ar}$ muscovite detrital mineral ages in metasediments for movement of the Torlesse suspect terrane around the eastern margin of Gondwanaland. *Terra Nova*, **10**, 183–189.
- BATT, G.E. & BRANDON, M.T. (2002) Lateral thinking: 2-D interpretation of thermochronology in convergent orogenic settings. *Tectonophysics*, **349**, 185–201.
- BEAUMONT, C., FULLSACK, P. & HAMILTON, J. (1994) Styles of crustal deformation in compressional orogens caused by subduction of the underlying lithosphere. *Tectonophysics*, **232**, 119–132.
- BERNET, M., BRANDON, M.T. & GARVER, J.I. (in press) Downstream changes in detrital zircon FT cooling ages in large modern rivers. *J. Sediment. Res.*
- BERNET, M., ZATTIN, M., GARVER, J.I., BRANDON, M.T. & VANCE, J.A. (2001) Steady-state exhumation of the European Alps. *Geology*, **29**, 35–38.
- BEVINGTON, P. & ROBINSON, K. (1992) *Data Reduction and Error Analysis for the Physical Sciences*. WCB/McGraw-Hill, San Francisco.
- BLOOM, A. (1998) *Geomorphology. A Systematic Analysis of Late Cenozoic Landforms*. Prentice Hall, Upper Saddle River.
- BRANDON, M.T. (1992) Decomposition of fission-track grain-age distributions. *Am. J. Sci.*, **292**, 535–564.
- BRANDON, M.T. (1996) Probability density plot for fission-track grain-age samples. *Radiation Measurements*, **26**, 663–676.
- BRANDON, M.T. (2002) Decomposition of mixed grain-age distributions using BINOMFIT. *On Track*, **24**, 13–18.
- BRANDON, M.T. & VANCE, J.A. (1992) Fission-track ages of detrital zircon grains: implications for the tectonic evolution of the Cenozoic Olympic subduction complex. *Am. J. Sci.*, **292**, 565–636.
- BROWN, E.T., STALLARD, R.F., LARSEN, M.C., RAISBECK, G.M. & YIOU, F. (1995) Denudation rates determined from the accumulation of in situ-produced ^{10}Be in the Luquillo experimental forest, Puerto Rico. *Earth Planet. Sci. Lett.*, **129**, 193–202.
- BROZOVIĆ, N., BURBANK, D.W. & MEIGS, A.J. (1997) Climatic limits on landscape development in the northwestern Himalaya. *Science*, **276**, 571–574.
- BURBANK, D.W. (2002) Rates of erosion and their implications for exhumation. *Mineral. Mag.*, **66**, 25–52.
- BURBANK, D.W., LELAND, J., FIELDING, E., ANDERSON, R.S., BROZOVIĆ, N., REID, M.R. & DUNCAN, C. (1996) Bedrock incision, rock uplift and threshold hillslopes in the northwestern Himalayas. *Nature*, **379**, 505–510.
- BURCHFIEL, B.D., ZHILENG, C., HODGES, K.V., YUPING, L., ROYDEN, L.H., CHANGRONG, D. & JIENE, X. (1992) The South Tibetan detachment system, Himalayan orogen: extension contemporaneous with and parallel to shortening in a collisional mountain belt. *Geol. Soc. Am. Spec. Pap.*, **269**, 1–41.
- CATLOS, E.J., HARRISON, T.M., KOHN, M.J., GROVE, M., RYERSON, F.J., MANNING, C.E. & UPRETI, B.N. (2001) Geochronologic and thermobarometric constraints on the evolution of the Main Central Thrust, central Nepal Himalaya. *J. Geophys. Res.*, **106**, 16,177–16,204.
- CERVENY, P.F., NAESER, N.D., ZEITLER, P.K., NAESER, C.W. & JOHNSON, N.M. (1988) History of uplift and relief of the Himalaya during the past 18 million years; evidence from sandstones of the Siwalik Group. In: *New Perspectives in Basin Analysis* (Ed. by K.L. Kleinspehn & C. Paola), pp. 43–61. Springer-Verlag, New York.
- COLCHEN, M., LEFORT, P. & PÊCHER, A. (1986) *Annapurna–Manaslu–Ganesh Himal*. Centre National de la Recherche Scientifique, Paris.
- COLEMAN, M.E. (1996) Orogen-parallel and orogen-perpendicular extension in the central Nepalese Himalayas. *Geol. Soc. Am. Bull.*, **108**, 1594–1607.
- COLEMAN, M.E. & HODGES, K.V. (1995) Evidence for Tibetan plateau uplift before 14 Myr ago from a new minimum age for east-west extension. *Nature*, **374**, 49–52.
- COPELAND, P. & HARRISON, M.T. (1990) Episodic rapid uplift in the Himalaya revealed by $^{40}\text{Ar}/^{39}\text{Ar}$ analysis of detrital K-feldspar and muscovite, Bengal fan. *Geology*, **18**, 354–359.
- COPELAND, P., HARRISON, T.M., HODGES, K.V., MARUEJOL, P., LEFORT, P. & PECHER, A. (1991) An early Pliocene thermal disturbance of the Main Central Thrust, central Nepal: implications for Himalayan tectonics. *J. Geophys. Res.*, **96**, 8475–8500.
- COPELAND, P., HARRISON, T.M. & LEFORT, P. (1990) Age and cooling history of the Manaslu granite: implications for Himalayan tectonics. *J. Volcanol. Geother. Res.*, **44**, 33–50.
- DODSON, M. (1973) Closure temperature in cooling thermochronological and petrological systems. *Contrib. Mineral. Petrol.*, **40**, 259–274.
- EDWARDS, R.M. (1995) $^{40}\text{Ar}/^{39}\text{Ar}$ geochronology of the Main Central Thrust (MCT) region: evidence for Late Miocene to Pliocene disturbances along the MCT, Marsyandi River valley, west-central Nepal Himalaya. *J. Nepal Geol. Soc.*, **10**, 41–46.
- FLETCHER, C.A.J. (1991) *Computational Techniques for Fluid Dynamics*. Springer Verlag, New York.

- FOWLER, C.M.R. (1990) *The Solid Earth, an Introduction to Geophysics*. Cambridge University Press, Cambridge.
- GARVER, J.I. & BRANDON, M.T. (1994) Fission-track ages of detrital zircons from Cretaceous strata, southern British Columbia: implications for the Baja BC hypothesis. *Tectonics*, **13**, 401–420.
- GARVER, J.I., BRANDON, M.T., RODEN-TICE, M. & KAMP, P.J.J. (1999) Exhumation history of orogenic highlands determined by detrital fission-track thermochronology. *Geol. Soc. Spec. Publ.*, **154**, 283–304.
- HARRISON, T.M., RYERSON, F.J., LE FORT, P., YIN, A., LOVERA, O.M. & CATLOS, E.J. (1997) A late Miocene-Pliocene origin for the central Himalayan inverted metamorphism. *Earth Planet. Sci. Lett.*, **146**, E1–E7.
- HENRY, P., LE PICHON, X. & GOFFÉ, B. (1997) Kinematic, thermal and petrological model of the Himalayas: constraints related to metamorphism within the underthrust Indian crust and topographic elevation. *Tectonophysics*, **273**, 31–56.
- HODGES, K. & BOWRING, S. (1995) $^{40}\text{Ar}/^{39}\text{Ar}$ thermochronology of isotopically zoned micas: insights from the southwestern USA Proterozoic orogen. *Geochim. Cosmochim. Acta*, **59**, 3205–3220.
- HODGES, K.V. (1998) $^{40}\text{Ar}/^{39}\text{Ar}$ thermochronology using the laser microprobe. In: *Reviews in Economic Geology 7: Applications of Microanalytical Techniques to Understanding Mineralizing Processes* (Ed. by M.A. McKibben & W.C. Shanks), pp. 53–72. Society of Economic Geologists, Tuscaloosa.
- HODGES, K.V. (2000) Tectonics of the Himalaya and southern Tibet from two perspectives. *Geol. Soc. Am. Bull.*, **112**, 324–350.
- HODGES, K.V., RUHL, K., WHIPPLE, K.X. & WOBUS, C. (2002) History of the Main Central Thrust system in the Marsyandi valley, central Nepal: evidence for steady-state orogenesis in the Himalaya? *Geol. Soc. Am. Abstr. Programs*, **34**, 411.
- HURFORD, A.J. & CARTER, A. (1991) The role of fission track dating in discrimination of provenance. *Geol. Soc. Spec. Publ.*, **57**, 67–78.
- KOOI, H. & BEAUMONT, C. (1996) Large-scale geomorphology: classical concepts reconciled and integrated with contemporary ideas via a surface processes model. *J. Geophys. Res.*, **101**, 3361–3386.
- KROGH, T.E. & KEPPIE, J.D. (1987) Detrital zircon ages indicating a North African provenance for the Goldenville Formation of Nova Scotia. In: *Mines and Minerals Branch Report of Activities* (Ed. by J.L. Bates & D.R. MacDonald), pp. 208. Department of Mines and Energy, Halifax.
- LAVÉ, J. & AVOUAC, J.P. (2001) Fluvial incision and tectonic uplift across the Himalaya of Central Nepal. *J. Geophys. Res.*, **106**, 26,561–26,591.
- MACFARLANE, A.M. (1993) Chronology of tectonic events in the crystalline core of the Himalaya, Langtang National Park, central Nepal. *Tectonics*, **12**, 1004–1025.
- MACFARLANE, A.M., HODGES, K.V. & LUX, D. (1992) A structural analysis of the Main Central Thrust zone, Langtang National Park, central Nepal. *Geol. Soc. Am. Bull.*, **104**, 1389–1402.
- MANCKTELOW, N.S. & GRASEMANN, B. (1997) Time-dependent effects of heat advection and topography on cooling histories during erosion. *Tectonophysics*, **270**, 167–195.
- MCGOLDRICK, P.J. & GLEADOW, A.J.W. (1978) Fission-track dating of lower Palaeozoic sandstones at Tatong, North central Victoria. *J. Geol. Soc. Aust.*, **24**, 461–464.
- MOLNAR, P. & ENGLAND, P. (1990) Late Cenozoic uplift of mountain ranges and global climatic change: chicken or egg? *Nature*, **346**, 29–34.
- MONTGOMERY, D.R. (2001) Slope distributions, threshold hillslopes, and steady-state topography. *Am. J. Sci.*, **301**, 432–454.
- MONTGOMERY, D.R. & BRANDON, M.T. (2002) Topographic controls on erosion rates in tectonically active mountain ranges. *Earth Planet. Sci. Lett.*, **201**, 481–489.
- NAJMAN, Y.M.R., PRINGLE, M.S., JOHNSON, M.R.W., ROBERTSON, A.H.F. & WIJBRANS, J.R. (1997) Laser $^{40}\text{Ar}/^{39}\text{Ar}$ dating of single detrital muscovite grains from early foreland-basin sedimentary deposits in India: implications for early Himalayan erosion. *Geology*, **25**, 535–538.
- OHMORI, H. (1992) Morphological characteristics of the scar created by large-scale rapid mass movement. *Jpn. Geomorphol. Union Trans.*, **13**, 185–202.
- PRATT, B., BURBANK, D.W., HEIMSATH, A. & OJHA, T. (2002) Impulsive alluviation during early Holocene strengthened monsoons, central Nepal Himalaya. *Geology*, **30**, 911–914.
- PRESS, W., TEUKOLSKY, S., VETTERLING, W. & FLANNERY, B. (1992) *Numerical Recipes in Fortran: the Art of Scientific Computing*. Cambridge University Press, Cambridge.
- ROBINSON, D.M., DECELLES, P.G., GARZIONE, C.N., PEARSON, O.N., HARRISON, T.M. & CATLOS, E.J. (2003) Kinematic model for the Main Central thrust in Nepal. *Geology*, **31**, 359–362.
- ROBINSON, D.M.D., PATCHETT, P.J. & GARZIONE, C.N. (2001) The kinematic evolution of the Nepalese Himalaya interpreted from Nd isotopes. *Earth Planet. Sci. Lett.*, **192**, 507–521.
- SEEBER, L. & GORNITZ, V. (1983) River profiles along the Himalayan arc as indicators of active tectonics. *Tectonophysics*, **92**, 335–367.
- STOCK, J.D. & MONTGOMERY, D.R. (1996) Estimating palaeorelief from detrital mineral age ranges. *Basin Res.*, **8**, 317–328.
- STÜWE, K. & HINTERMÜLLER, M. (2000) Topography and isotherms revisited: the influence of laterally migrating drainage divides. *Earth Planet. Sci. Lett.*, **184**, 287–303.
- STÜWE, K., WHITE, L. & BROWN, R. (1994) The influence of eroding topography on steady-state isotherms: application to fission track analysis. *Earth Planet. Sci. Lett.*, **124**, 63–74.
- VANNAY, J.C. & HODGES, K.V. (1996) Tectonometamorphic evolution of the Himalayan metamorphic core between Annapurna and Dhaulagiri, central Nepal. *J. Metamorphic Geol.*, **14**, 635–656.
- WHIPPLE, K.E., KIRBY, E. & BROCKLEHURST, S.H. (1999) Geomorphic limits to climate-induced increases in topographic relief. *Nature*, **401**, 39–43.
- WHITE, N.M., PRINGLE, M., GARZANTI, E., BICKLE, M., NAJMAN, Y., CHAPMAN, H. & FRIEND, P. (2002) Constraints on the exhumation and erosion of the High Himalayan Slab, NW India, from foreland basin deposits. *Earth Planet. Sci. Lett.*, **195**, 29–44.
- WILLETT, S.D. (1999) Orogeny and orography: the effects of erosion on the structure of mountain belts. *J. Geophys. Res.*, **104**, 28,957–28,982.
- WILLETT, S.D. & BRANDON, M.T. (2002) On steady states in mountain belts. *Geology*, **30**, 175–178.
- WILLETT, S.D., SLINGERLAND, R. & HOVIUS, N. (2001) Uplift, shortening, and steady state topography in active mountain belts. *Am. J. Sci.*, **301**, 455–485.
- YAMANAKA, H. & IWATA, S. (1982) River terraces along the middle Kali Gandaki and Marsyandi Khola, central Nepal. *J. Nepal Geol. Soc.*, **2**, 95–112.
- ZHANG, P., MOLNAR, P. & DOWNS, W.R. (2001) Increased sedimentation rates and grain sizes 2–4 Myr ago due to the influence of climate change on erosion rates. *Nature*, **410**, 891–897.

Manuscript accepted 25 June 2003